Hindawi Publishing Corporation
International Journal of Antennas and Propagation
Volume 2013, Article ID 475375, 8 pages
http://dx.doi.org/10.1155/2013/475375

Research Article

A mm-Wave 2D Ultra-Wideband Imaging Radar for Breast Cancer Detection

Stefano Moscato,[1] Giulia Matrone,[1] Marco Pasian,[1] Andrea Mazzanti,[1] Maurizio Bozzi,[1] Luca Perregrini,[1] Francesco Svelto,[1] Giovanni Magenes,[1] Paolo Arcioni,[1] and Paul Summers[2]

[1] *Department of Electrical, Computer, and Biomedical Engineering, University of Pavia, Via Ferrata 1, 27100 Pavia, Italy*
[2] *Division of Oncology, IEO European Institute of Oncology, Via Ripamonte 435, 20141 Milano, Italy*

Correspondence should be addressed to Stefano Moscato; stefano.moscato01@universitadipavia.it

Received 10 May 2013; Revised 11 July 2013; Accepted 14 July 2013

Academic Editor: Tzyh-Ghuang Ma

This paper presents the preliminary design of a mm-wave ultra-wideband (UWB) radar for breast cancer detection. A mass screening of women for breast cancer is essential, as the early diagnosis of the tumour allows best treatment outcomes. A mm-wave UWB radar could be an innovative solution to achieve the high imaging resolution required without risks for the patient. The 20–40 GHz frequency band used in the system proposed in this work guarantees high cross/range resolution performances. The developed preliminary architecture employs two monomodal truncated double-ridge waveguides that act as antennas; these radiators are shifted by microstep actuators to form a synthetic linear aperture. The minimum antenna-to-antenna distance achievable, the width of the synthetic aperture, and the minimum frequency step determine the performance of the 2D imaging system. Measures are performed with a mm-wave vector network analyzer driven by an automatic routine, which controls also the antennas shifts. The scattering matrix is then calibrated and the delay-multiply-and-sum (DMAS) algorithm is applied to elaborate a high-resolution 2D image of the targets. Experimental results show that 3 mm cross and 8 mm range resolutions were achieved, which is in line with theoretical expectations and promising for future developments.

1. Introduction

Breast cancer ranks fifth overall as a cause of death from cancer and remains the most frequent cause of death due to cancer in women [1]. In the United States, for example, almost 6% of the population aged between 50 and 69 is affected by breast cancer [2]. However, if the cancer is detected early enough (in stages known as I or IIA), surgery to completely remove the tumour mass has a consequent 5-year survival rate of more than 80% [2]. X-ray mammography is the most commonly used technique for breast screening because of its high resolution and good performance in tumor detection. Unfortunately, due to the use of ionizing radiations, it is not without risks, particularly for women younger than 50 years old; it is very uncomfortable because it involves breast compression [3], and it is not failsafe; 23.8% of women screened in [4] had at least one false positive mammogram.

A mm-wave breast imaging system is a very attractive alternative: it is risk-free and more comfortable and can provide a resolution in the range of a few millimeters, suitable for a basic breast cancer imaging. With a central operating frequency around 30 GHz, in fact, it is possible to provide an adequate resolution, not achievable with lower frequencies, while maintaining an acceptable penetration in the human tissues, not achievable at higher frequencies (in the mm-wave range).

Microwave and mm-wave radar techniques detect discontinuities in the dielectric constant ε_r in the medium. In particular, a fraction of the power irradiated by the antenna system is reflected by the discontinuity back to the antenna system itself, and thus, the detection of the discontinuity position is possible. This methodology is also suitable for breast cancer detection; studies reported in [5] examined the electrical characteristic of human tissues. In particular, it is

evident that in the microwave region the ε_r of tumour tissue is approximately five times greater than that of fat.

The received signal is attenuated due to not only tissue propagation losses but also the limited backscattering of a target with small dimensions. Electronic circuitry requires strict constraints in terms of signal-to-noise ratio (SNR) in order to discern the scattered signal from the noise floor. Preliminary calculations [6], which take into account propagation losses within the human tissue and the expected ratio between incident and reflected power, indicate that the total signal power collected by a system composed of 7×7 antennas (Figure 1) can be estimated to be around −50 dBm, if 0 dBm is the power transmitted. Assuming a reasonable receiver noise figure (NF) of 10 dB and a receiver filter bandwidth B of 1 kHz, the total noise power N for a planar array of 49 antennas is given by

$$N = -173\,\text{dB} + 10\log(B) + \text{NF} + 10\log(49 \times 48 \times 20) = -87\,\text{dBm}, \quad (1)$$

where the first term is the noise floor at room temperature, the second is the noise collected within the filter bandwidth of 1 kHz, the third is the noise of each receiver, and the final term accounts for the integration of the noise along 20 frequency points for an array of 49 antennas. Therefore, a robust SNR of 37 dB is expected, and this is suitable for breast cancer detection.

In the last few years, the lower frequencies of the microwave band have been exploited in several prototypes to produce three-dimensional breast images. The most widely employed band for breast cancer imaging has a central frequency of 7 GHz with an average span of 10 GHz [7–13]. This band involves wavelengths down to few centimeters, which guarantees significant penetration of the electromagnetic field in human tissues. While microwave circuitry is simpler at lower frequencies, it becomes bulky and thus inconvenient for system integration. In addition, the relatively low frequency poses limitation on the achievable resolution.

In the literature, mm-wave radar imaging systems have already been proposed, including a 3D holographic microwave imaging technique [14], which operates in the 30 GHz band and a K-band radar system for nondestructive concrete testing [15]. Also E-band imaging systems have been developed, but their use is best suited for the detection of concealed weapons. In fact, a prototype with a working frequency from 72 to 80 GHz has been designed and tested for the detection of guns or knives under passengers clothes [16, 17]. This latter shows very accurate cross resolution (resolution perpendicular to the direction of propagation of the transmitted signal), but at these frequencies there is no penetration within human tissues. In addition, the low bandwidth used (8 GHz) leads to a very poor range resolution (resolution along the direction of propagation of the transmitted signal). For these reasons, this type of system is not suited for breast cancer detection.

The novel contribution of this work is the development of a mm-wave radar imaging system with a 20 GHz bandwidth centered at 30 GHz, which can be potentially employed for breast imaging and cancer detection. This band makes it possible to pursue both high range and cross resolutions with respect to existing systems and at the same time to achieve adequate penetration in the human tissues. Compared to other works employing the 20–40 GHz frequency band, we have also developed a preliminary system prototype and tested it in a real experimental scenario, so as to evaluate its performance and target detection capability. Moreover, mm-waves favour the development of a compact, highly integrated system. This is fundamental to develop a cost-effective system for medical screening among a vast segment of the population.

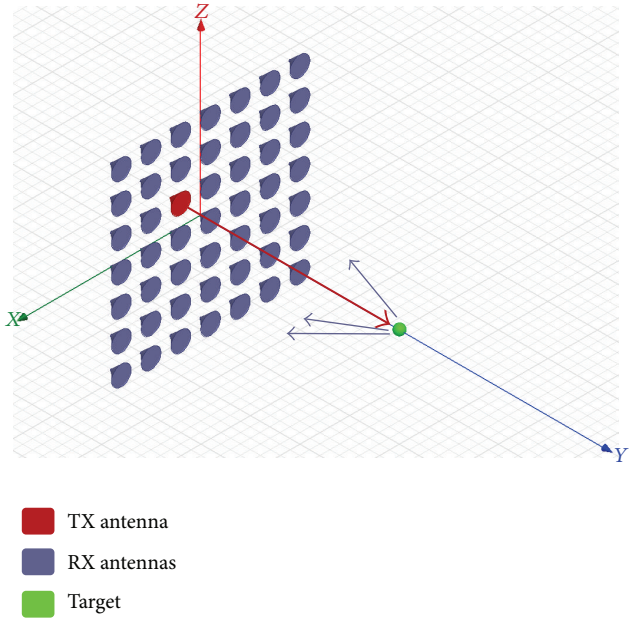

Figure 1: A schematic 7×7 antenna array.

In this paper, the design of a preliminary imaging system is presented. Instead of a complete system that includes a full planar array of antennas able to generate 3D images, this preliminary system is based on a synthetic aperture realized by two antennas for 2D imaging. Data collection used the reliable methodology of stepped frequency continuous wave (SFCW) radar. In particular, the data for image reconstruction were obtained by shifting the antennas along a predetermined line, parallel to the surface under investigation. In this way, an equivalent linear array of N radiators was investigated, and a 2D image (lateral displacement by vertical penetration) was obtained. Image reconstruction was based on the delay-multiply-and-sum (DMAS) algorithm, proposed in [18], which was selected for this application thanks to its good performance in terms of dynamic range.

For this preliminary system, the intended targets were synthetic objects in free space. This configuration allowed us to evaluate all the critical system aspects. In fact, a complete 3D imaging system, based on a planar array of $N \times M$ radiators, would only require larger computational resources and mechanical complexity. As said before, these aspects are expected to be solved thanks to the possibilities offered by mm-wave devices, which are suited to realizing a compact system in which the silicon-based integration

between radiators, electronic front end, and data processing can be exploited.

This paper is organized in five sections: in Section 2 the design of the experimental setup of the antenna array is presented, in Section 3 the imaging algorithm is discussed, Section 4 presents the results and a high resolution 2D image of a two-target dielectric scenario, and Section 5 concludes the paper by presenting the next steps required to develop a complete mm-wave breast cancer imaging system.

2. Design of the Stepped Frequency Continuous Wave Radar

The SFCW approach considers the antenna-target-antenna electromagnetic system as a linear transfer function, by defining its behaviour according to the measured scattering parameters. All the information about the target is obtained from the magnitude and phase of the transfer function between two antennas. The architecture of the synthetic antenna array (in particular the central working frequency and the aperture width) sets the performance of the imaging system in terms of cross resolution, while the frequency bandwidth (BW) sets the range resolution. Range resolution has been well studied in previous works [11, 17, 19, 20] and is proportional to the inverse of BW. Another feature is the nonambiguous range; since the acquisition of the scattering parameters (S parameters) is based on a finite number of frequencies, the quantization step sets the distance in time (and consequently in space) between each signal replica, called the nonambiguous range (R_{NA}). This means that only the portion of space between the origin and R_{NA} has a physical meaning. R_{NA} is simply calculated as $v/2\Delta f$, where v is the propagation speed in the medium and Δ_f is the frequency step. The prototype architecture described in this paper, for the detection of targets in air, has an R_{NA} of 300 mm.

The proposed 20 GHz bandwidth needs proper broadband antennas. In this preliminary design, the chosen radiators are two truncated double-ridge waveguides. Thanks to the double-ridge architecture, the cut-off frequency of the fundamental mode TE_{10} is lower than that for standard waveguides, with a consequent widening of the bandwidth. Thus, the radiators reach the desired bandwidth, operating from 18 GHz to 40 GHz. On the other hand, this type of antenna does not offer optimal input matching, that is, approximately −6 dB. However, this is not a problem for this prototype because the power budget provides a large margin. Better matching could be achieved by designing a proper matching section, if required.

The main difference between a standard radar and this system for breast cancer detection is the distance between the target and the antenna array. Biomedical applications, in fact, usually need a range of view, which is well below one meter. In particular, breast cancer imaging is limited by breast depth, which is usually on the order of a few centimeters when the patient is lying supine during the screening. Furthermore, the high working frequency (more than 20 GHz in this case) and the overall array aperture (on the order of some tens of centimeters) impose a near field region that extends up to several meters or even tens of meters [21]. This means that this system operates in the deep near field. Therefore, a standard design approach does not guarantee an optimal performance of the antenna array. Nevertheless, a convenient point to start the design of the synthetic array is the antenna-to-antenna spacing and radiators number N [21]. As in far field approach, the radiators distance is related to the presence of (generally unwanted) grating lobes. On the other hand, the −3 dB beamwidth is directly controlled by the total aperture width.

The maximum aperture available, limited by the experimental setup dimensions, is 200 mm. A number of possible architectures were investigated, but the best performance was reached with a linear array of 35 antennas with variable reciprocal spacings. Physically adjacent antennas spacing is limited to 25 mm by flange transition hindrance. Subsequent spacings, achieved with the employment of linear actuators, are reduced to 5 mm. This architecture guarantees high performance both in terms of resolution, due to the large total aperture, and in terms of grating lobes, which are avoided across the entire field of view. The expected cross resolution is 3 mm, calculated as the third part of the central frequency wavelength, and the range resolution is down to 8 mm, thanks to the large bandwidth employed. Another benefit of this architecture based on a high number of antennas is the increasing of process gain and consequently a low noise floor in the resulting image.

In the experimental setup, four microstep linear actuators were used to shift the antennas. Each pair of shifters was crossed, as shown in Figure 2, to allow two-dimensional movement of the antennas. In this way, the experimental setup can be extended to generate 3D images, though for this prototype the antenna movements were limited to a single line and generated 2D images, as discussed in the previous section. The measurements are directed to a mm-wave vector network analyzer (VNA) that acquires the transmission S-parameters of the antenna-target-antenna system over the frequency band of interest. Radiators were fastened to the carriage of linear actuators using the holes of the flanges and connected to the VNA cables with coaxial K-1.85 mm male-female transitions. Antennas were directed towards the floor, and the measurement environment was totally surrounded by anechoic panels, as illustrated in Figures 3 and 4.

The VNA and linear shifters were connected to a personal computer, where a LabVIEW routine automatically coordinated antenna movement and the sequential measurements. The described architecture considers each antenna as a transmitter when all the other radiators receive the scattered signals. For an array of N antennas then there are N^2 pairs of antennas for which a VNA measurement is required. Since this design is based on 35 antennas, 1225 measurements are needed. However, considering the symmetry of the scattering matrix, each measurement with a single pair of antennas could be used twice, and the number of measurements actually performed drastically decreased to 630, saving the total time of measure.

The signal scattered from targets is very weak, and the ratio between the received wave and the transmitted one easily reaches values lower than −70 dB. In addition, two different problems affect the scattered signal reception. First, the

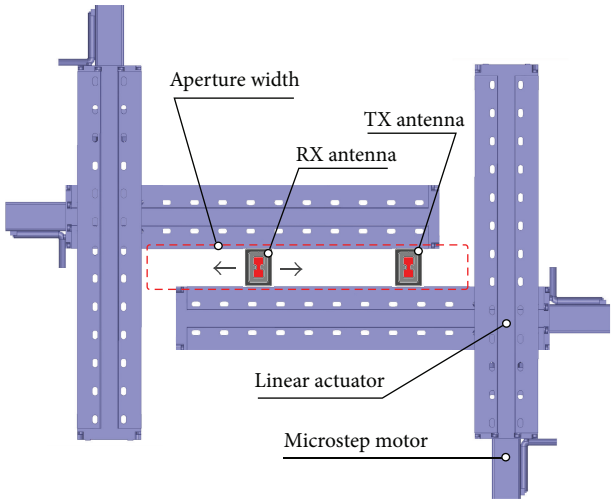

FIGURE 2: Schematic top view of the setup. The red dashed line identifies the total width of the synthetic array. The grey arrows sketch the RX antenna movements.

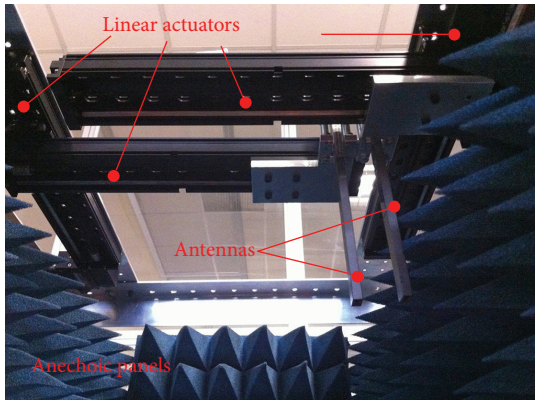

FIGURE 3: Lateral view of the setup.

small antenna spacings generate a large mutual coupling, also known as crosstalk (XT). Second, the phase of the received signals is affected by several external factors (e.g., waveguide propagation and spurious backscattering), and this further deteriorates the quality of the received signal. XT is easily suppressed by two consecutive measurements, one with and one without the targets, in order to calibrate the imaging system and suppress antennas coupling and environment multiple reflections. Then, the correct phase of the received signal is achieved with a known calibration standard. In particular, a copper plane is placed in front of the antennas at a known position and its scattering matrix is measured. A copper plane is suitable as a calibration standard (such as a short termination) because its S-matrix, called H_τ, is known analytically. In addition to the magnitude, the phase delay introduced by the metal plane is strictly related to its distance from the antennas. Each element of H_τ is the complex number $\exp(-j2\pi f\tau)$, estimated for each frequency f and for each pair of antennas, which determines the propagation path and, therefore, the time delay τ. The ratio between analytical

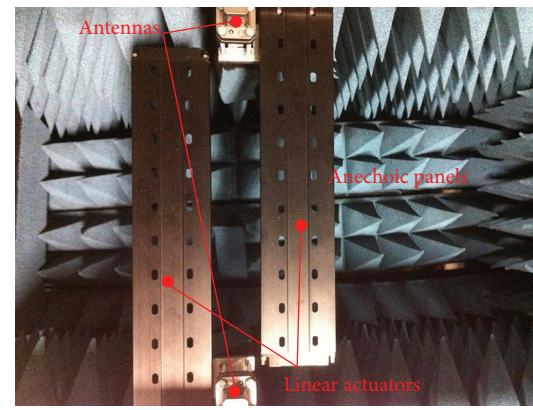

FIGURE 4: Top view of the setup.

and measured S-matrices is the two-way transfer function of microwave circuitry (cables, transitions, and antennas). The equation that summarizes the entire calibration process is stated below:

$$H_{\text{target}} = \frac{(H_A H_S H_A + H_A H_{\text{XT}} H_A) - (H_A H_{\text{XT}} H_A)}{H_\tau / H_{\text{plane}}}. \quad (2)$$

In this equation, H_{target} is the calibrated transfer function of the scenario, H_A is the antenna response, H_S is the scattering transfer function, and H_{XT} is the frequency domain crosstalk contribution. Finally, H_{plane} is the measurement of the calibration standard.

A simple example of antennas postprocessing calibration is shown in Figures 5 and 6. The one-dimensional (range) response of a 2 mm dielectric target, placed at 110 mm from the antennas array, is plotted in both figures. Figure 5 shows the received signal without antennas calibration: the main peak spreads over several millimeters, the target distance is misrepresented, and the noise floor is very high. On the other hand, when antenna calibration is applied, as shown in Figure 6, the main peak is sharp and matches the correct target distance with a visible lowering of the noise floor.

When dealing with a real scenario however, artifacts due to air-skin reflections will also need to be considered during the calibration process. Ideally, the system design should allow matching between the antenna array and the breast skin (i.e., through a dielectric coupling medium). Then, other signal postprocessing techniques (e.g., subtracting the average of the received signals or time gating) could be applied to further remove these artifacts.

3. Image Formation

The multistatic DMAS algorithm, originally conceived in [18] for microwave breast imaging, was used for image reconstruction. Among other algorithms proposed in the literature (e.g., back-propagation [17, 22], Kirchhoff [23] and range migration [24], delay-and-sum (DAS) [25], microwave imaging via space-time (MIST) beamforming [26], or adaptive beamforming methods [27]), the DMAS allows for achieving a better SNR and dynamic range [18, 28], but at the expense of

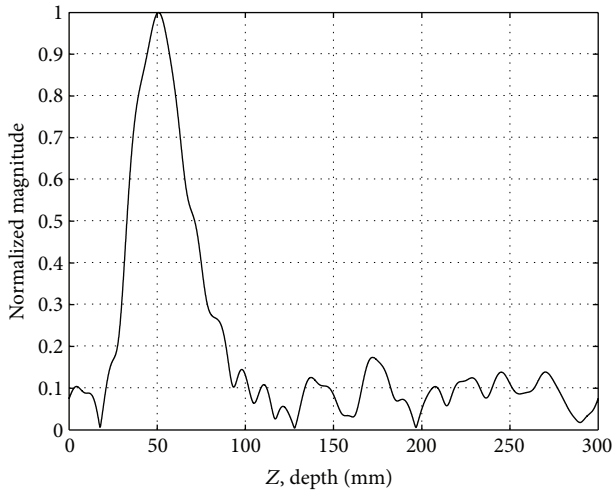

Figure 5: Received signal without calibration.

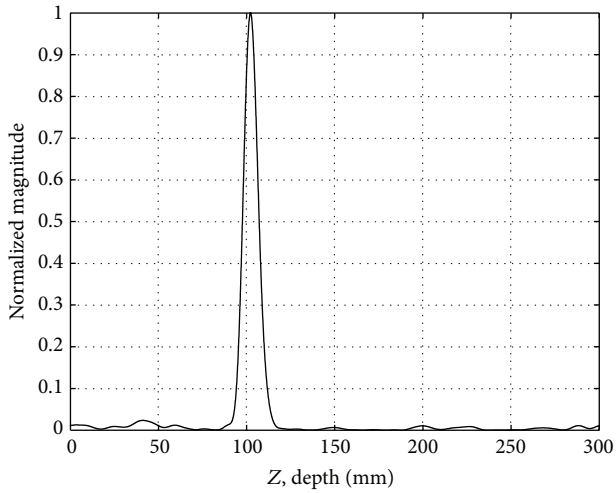

Figure 6: Calibrated received signal.

an increased number of operations and longer computational times. This may indeed be a critical issue for future real-time implementations or 3D reconstruction, where the data to be processed will scale quadratically with the linear dimension of the array.

The first operation is to obtain backscattered signals by convolving the measured scattering coefficients matrix with the input excitation signal, that is, a 30 GHz modulated Gaussian pulse:

$$p_{\mathrm{TX}}(t) = A_0 e^{-t^2/\sigma^2}, \tag{3}$$

where A_0 controls pulse amplitude and σ is 34.15 ps (BW = 20 GHz). These are synthetically focused on each focal point in the considered space. The two-way propagation time t_{2W}—that is, the time spent to cover the distance from the transmitting antenna to the focal point (t_T) and back to the receiving antenna (t_R)—is computed for each antenna pair ($t_{2W} = t_T + t_R$) and used to realign the received signals. This way, the image intensity at each focal point (pixel) is obtained by employing the received signals amplitudes at the corresponding t_{2W} time instant. The DMAS algorithm involves pairing multiplications of these values for each focal point, which are then summed and squared. The image is finally obtained after envelope detection, intensities normalization, and log compression.

Some indices of the imaging system performance can be derived by plotting its characteristic point spread function (PSF) over the scan plane, which allows for evaluating resolution and side lobes entity. The PSF was computed by simulating a 35-antenna linear array and a single-point scatterer placed on the array central axis at a depth of 110 mm. Image reconstruction was performed by the DMAS algorithm. In Figure 7, three different views of two-way PSF are represented. As the PSF shows, the cross resolution (at −3 dB) of the developed system is ~3 mm (Figure 7(b)), while range resolution is ~9 mm (Figure 7(c)). The results achieved are close to those expected for both resolutions. Moreover, Figure 7 highlights that with the DMAS algorithm a high dynamic range and enhanced contrast can be achieved, since side lobes and average noise floor are significantly lowered with respect to the main lobe.

4. Experimental Results

The results achieved with the architecture described in Section 2 are presented for a test bench that was arranged in order to highlight the capabilities of the proposed system.

Two little fragments of corrugated paper were chosen as targets and placed 110 mm far from the radiators array. Targets with low hindrance and low dielectric contrast were intentionally selected to limit scattering. This way, it is possible to have a weak received signal, thus imitating the expected conditions for the target application, where the received power is limited by propagation within the human breast tissue.

Each target had a cylindrical shape with a lower than 2 mm diameter, near to the expected resolution limit. The dielectric constant ε_r was estimated to be around 2.5, based on measurements in a resonator using standard techniques. Figure 8 shows the experimental setup.

Figure 9 represents the 2D image of the considered scenario, obtained by using the DMAS algorithm. The DMAS was implemented in Matlab (The MathWorks, Natick, MA, USA) and took about 15 minutes to reconstruct this 200 × 200 pixel image, running on an Intel i7 processor. The long computational time is expected to decrease when the algorithm is implemented on a dedicated hardware.

The targets are well identified and their positions are detected with a millimeter accuracy. The high resolution image confirms the main properties of the designed architecture: the capability to detect targets down to a 2 mm diameter, a very high dynamic range with a noise floor down to −60 dB, and a less than 10 mm range resolution (at −3 dB), according to theory assumptions.

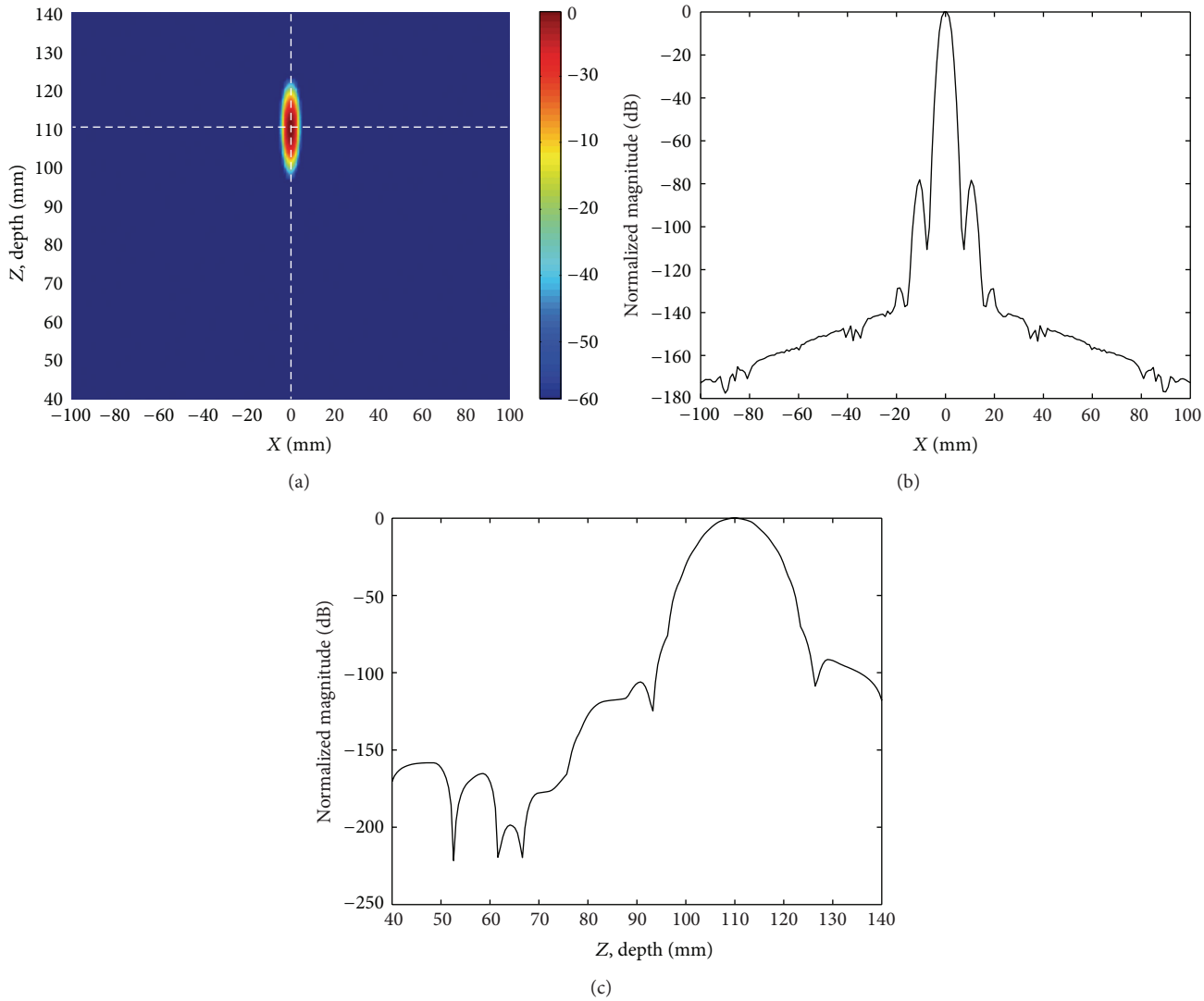

Figure 7: Two-way PSF: (a) on the xz plane (magnitude scale is in dB; the dynamic range used for PSF representation is 60 dB); (b) profile at a 110 mm depth, that is, along the horizontal dashed white line depicted in (a); (c) profile along the range axis ($x = 0$), that is, along the vertical dashed white line depicted in (a). The antenna linear array is aligned along the x-axis and centered at the origin of the reference system.

Some further considerations may be made on the obtained results. The range resolution, in terms of millimeters, is actually expected to decrease (i.e., to improve) when working in breast tissue, due to its dielectric coefficient which is almost 5 times higher than that in air. In that case the resolution would be about 3 mm, which fits these application requirements. In order to improve the range resolution in terms of wavelengths however, the antenna bandwidth will need to be broadened, but this would lead to a more complex and expensive system.

5. Conclusion and Future Developments

In this paper a mm-wave UWB radar for breast imaging is presented, and a preliminary 2D high-resolution measurement is described. The innovative contribution of this work derives from the frequency range employed, that is, from 20 GHz to 40 GHz, and for the total bandwidth of the system, that is, 20 GHz. These features, should allow a higher resolution to be achieved to already existing systems, while providing adequate penetration in the human tissues for breast imaging applications. The experimental results obtained by employing the prototype in a real scenario show, a cross resolution down to 3 mm with a range resolution of 8 mm. Moreover, the measurements also show a very high dynamic range, around 60 dB, thanks to the large number of antennas (i.e., 35) implemented in this preliminary prototype by synthetic aperture.

The presented results are promising, and they will serve as the baseline for the development of a full 3D breast imaging system.

To employ a high-frequency band implies the reduction of microwave circuitry hindrance, and this is fundamental to develop a cost-effective system aimed at a widespread

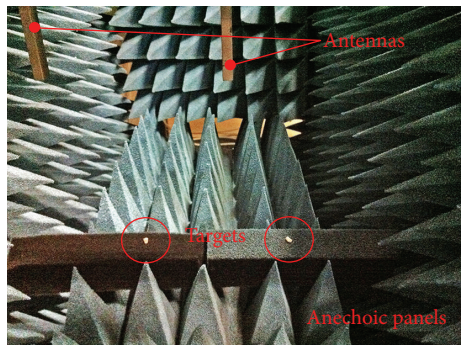

Figure 8: Measurement scenario: lateral view. The targets are the white dots placed on an anechoic base.

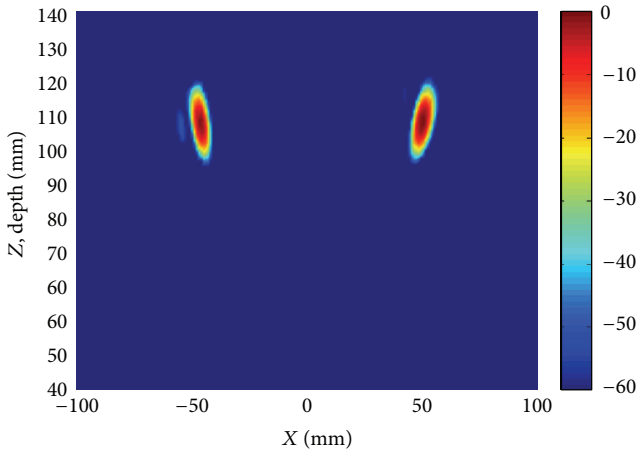

Figure 9: Final image of two small dielectric spheres at 110 mm from the antennas. Magnitude scale is in dB (dynamic range = 60 dB).

use in population screening. In particular, UWB antennas and integrated transmission lines, for example, based on the innovative structures of substrate integrated waveguide (SIW) [29], can be designed on the same silicon substrate of CMOS transmitters and receivers. This allows for a convenient manufacturing of a dense two-dimensional array with integrated CMOS circuitry. High working frequencies and high number of antennas need also a speedup in TX and RX architectures. This point is partially solved nowadays with the state-of-the-art CMOS lithography, with a channel length down to tens of nanometers, but further studies on innovative front-end architectures are required.

Other future developments are foreseen, which will be focused on the application of the proposed prototype system in a more realistic scenario and on the design of a dedicated hardware (e.g., FPGA device) for a significant speedup of signal processing and image formation algorithms.

References

[1] "International Agency for Research on Cancer," http://globocan.iarc.fr/.

[2] "National Cancer Institute at the National Institutes of Health," http://www.cancer.gov/.

[3] E. C. Fear, P. M. Meaney, and M. A. Stuchly, "Microwaves for breast cancer detection?" *IEEE Potentials*, vol. 22, no. 1, pp. 12–18, 2003.

[4] J. G. Elmore, M. B. Barton, V. M. Moceri, S. Polk, P. J. Arena, and S. W. Fletcher, "Ten-year risk of false positive screening mammograms and clinical breast examinations," *The New England Journal of Medicine*, vol. 338, no. 16, pp. 1089–1096, 1998.

[5] X. Li, S. K. Davis, S. C. Hagness, D. W. Van der Weide, and B. D. Van Veen, "Microwave imaging via space-time beamforming: experimental investigation of tumor detection in multilayer breast phantoms," *IEEE Transactions on Microwave Theory and Techniques*, vol. 52, no. 8, pp. 1856–1865, 2004.

[6] R. E. Collins, *Foundations For Microwave Engineering*, McGraw-Hill, 1966.

[7] M. Klemm, I. J. Craddock, J. A. Leendertz, A. Preece, and R. Benjamin, "Radar-based breast cancer detection using a hemispherical antenna array: experimental results," *IEEE Transactions on Antennas and Propagation*, vol. 57, no. 6, pp. 1692–1704, 2009.

[8] M. E. Bialkowski, A. M. Abbosh, Y. Wang, D. Ireland, A. A. Bakar, and B. J. Mohammed, "Microwave imaging systems employing cylindrical, hemispherical and planar arrays of ultrawideband antennas," in *Proceedings of the Asia-Pacific Microwave Conference (APMC '11)*, pp. 191–194, Melbourne, Australia, December 2011.

[9] M. E. Bialkowski, "Ultra wideband microwave system with novel image reconstruction strategies for breast cancer detection," in *Proceedings of the 40th European Microwave Conference*, pp. 537–540, Paris, France, September 2010.

[10] M. O'Halloran, E. Jones, and M. Glavin, "Quasi-multistatic MIST beamforming for the early detection of breast cancer," *IEEE Transactions on Biomedical Engineering*, vol. 57, no. 4, pp. 830–840, 2010.

[11] M. Bassi, A. Bevilacqua, A. Gerosa, and A. Neviani, "Integrated SFCW transceivers for UWB breast cancer imaging: architectures and circuit constraints," *IEEE Transactions on Circuits and Systems*, vol. 59, no. 6, pp. 1228–1241, 2012.

[12] B. Yang, A. G. Yarovoy, and L. P. Ligthart, "UWB stacked patch antenna design for near-field imaging radar antenna array," in *Proceedings of the 3rd European Conference on Antennas and Propagation (EuCAP '09)*, pp. 817–821, Berlin, Germany, March 2009.

[13] N. K. Nikolova, "Microwave imaging for breast cancer," *IEEE Microwave Magazine*, vol. 12, no. 7, pp. 78–94, 2011.

[14] R. K. Amineh, M. Ravan, A. Khalatpour, and N. K. Nikolova, "Three-dimensional near-field microwave holography using reflected and transmitted signals," *IEEE Transactions on Antennas and Propagation*, vol. 59, no. 12, pp. 4777–4789, 2011.

[15] S. Kharkovsky, J. T. Case, M. T. Ghasr, R. Zoughi, S. W. Bae, and A. Belarbi, "Application of microwave 3D SAR imaging technique for evaluation of corrosion in steel rebars embedded in cement-based structures," in *Proceedings of the AIP Conference Proceedings*, vol. 1430, pp. 1516–1523, 2012.

[16] A. Schiessl, S. S. Ahmed, A. Genghammer, and L.-P. Schmidt, "A technology demonstrator for a 0.5 m × 0.5 m fully electronic digital beamforming mm-Wave imaging system," in *Proceedings of the 5th European Conference on Antennas and Propagation (EUCAP '11)*, pp. 2606–2609, Rome, Italy, April 2011.

[17] S. S. Ahmed, A. Schiessl, and L.-P. Schmidt, "A novel fully electronic active real-time imager based on a planar multistatic

sparse array," *IEEE Transactions on Microwave Theory and Techniques*, vol. 59, no. 12, pp. 3567–3576, 2011.

[18] H. B. Lim, N. T. Nhung, E. P. Li, and N. D. Thang, "Confocal microwave imaging for breast cancer detection: delay-multiply-and-sum image reconstruction algorithm," *IEEE Transactions on Biomedical Engineering*, vol. 55, no. 6, pp. 1697–1704, 2008.

[19] D. M. Sheen, D. L. McMakin, and T. E. Hall, "Three-dimensional millimeter-wave imaging for concealed weapon detection," *IEEE Transactions on Microwave Theory and Techniques*, vol. 49, no. 9, pp. 1581–1592, 2001.

[20] X. Zhuge and A. G. Yarovoy, "A sparse aperture MIMO-SAR-based UWB imaging system for concealed weapon detection," *IEEE Transactions on Geoscience and Remote Sensing*, vol. 49, no. 1, pp. 509–518, 2011.

[21] C. A. Balanis, *Antenna Theory: Analysis and Design*, John Wiley and Sons, 1997.

[22] S. S. Ahmed, A. Schiess, and L.-P. Schmidt, "Multistatic mm-wave imaging with planar 2D-arrays," in *Proceedings of the German Microwave Conference (GeMIC '09)*, Munich, Germany, March 2009.

[23] X. Zhuge, T. G. Savelyev, A. G. Yarovoy, L. P. Ligthart, and B. Levitas, "Comparison of different migration techniques for UWB short-range imaging," in *Proceedings of the 6th European Radar Conferenc*, pp. 184–187, Amsterdam, The Netherlands, October 2009.

[24] X. Zhuge and A. G. Yarovoy, "Three-dimensional near-field MIMO array imaging using range migration techniques," *IEEE Transactionson Image Processing*, vol. 21, no. 6, pp. 3026–3033, 2012.

[25] E. C. Fear, X. Li, S. C. Hagness, and M. A. Stuchly, "Confocal microwave imaging for breast cancer detection: localization of tumors in three dimensions," *IEEE Transactions on Biomedical Engineering*, vol. 49, no. 8, pp. 812–822, 2002.

[26] E. J. Bond, X. Li, S. C. Hagness, and B. D. Van Veen, "Microwave imaging via space-time beamforming for early detection of breast cancer," *IEEE Transactions on Antennas and Propagation*, vol. 51, no. 8, pp. 1690–1705, 2003.

[27] Y. Xie, B. Guo, L. Xu, J. Li, and P. Stoica, "Multistatic adaptive microwave imaging for early breast cancer detection," *IEEE Transactions on Biomedical Engineering*, vol. 53, no. 8, pp. 1647–1657, 2006.

[28] E. Kirshin, G. K. Zhu, M. Popovich, and M. Coates, "Evaluation of the mono-static microwave radar algorithms for breast imaging," in *Proceedings of the 5th European Conference on Antennas and Propagation (EUCAP '11)*, pp. 881–885, Rome, Italy, April 2011.

[29] R. Garg, I. Bahl, and M. Bozzi, *Microstrip Lines and Slotlines*, Artech House, 2013.